

Cell Tracing Dyes Significantly Change Single Cell Mechanics

Valentin Lulevich,[†] Yi-Ping Shih,[‡] Su Hao Lo,[‡] and Gang-yu Liu^{*,†}

Department of Chemistry, University of California, Davis, California 95616, and Department of Biochemistry and Molecular Medicine, Center for Tissue Regeneration and Repair, University of California—Davis, Sacramento, California 95817

Received: November 24, 2008; Revised Manuscript Received: March 15, 2009

Cell tracing dyes are very frequently utilized in cellular biology research because they provide highly sensitive fluorescent tags that do not compromise cellular functions such as growth and proliferation. In many investigations concerning cellular adhesion and mechanics, fluorescent dyes have been employed with the assumption of little impact on the results. Using the single cell compression technique developed by our team, the single cell mechanics of MDA-MB-468 and MLC-SV40 cells were investigated as a function of dye uptake. Cell tracing dyes increase living cell stiffness 3–6 times and cell-to-probe adhesion up to 7 times. These results suggest a more significant effect than toxins, such as thrombin. A simple analytical model was derived to enable the extraction of the Young's moduli of the cell membrane and cytoskeleton from the force–deformation profiles measured for individual cells. The increase in Young's modulus of the membrane is 3–7 times, which is more significant than that of the cytoskeleton (1.1–3.4 times). We propose that changes in cell mechanics upon the addition of fluorescent tracing dye are primarily due to the incorporation of amphiphilic dye molecules into the cellular plasma membrane, which increases the lateral interaction among phospholipid chains and thus enhances their rigidity and adhesion.

Introduction

Fluorescent dyes for living cells, i.e., cell tracing dyes, play an important role in cellular biology research by identifying cell viability and revealing cytotoxicity,^{1,2} following proliferation,³ and monitoring cell adhesion and spreading.^{4,5} These dyes are also used for quantification of cellular membrane permeability,^{6,7} as well as for tests of drug resistance.⁸ Typically, only specific intracellular enzymes can activate the fluorescence by changing dyes' molecular structure (e.g., increasing conjugation). As a result, cells exhibit bright fluorescent signals in contrast to the nonfluorescent media.^{9,10} Upon passing through the cellular membrane and entering the cell, some dye molecules are localized within the cell by attachment to cellular proteins.¹¹ At low concentrations, cell tracing dyes are considered noncytotoxic because dye-treated cells continue to proliferate and pass multiple division cycles.³ However, the impact of cell tracing dyes on cell stiffness and adhesion has not yet known nor been systematically investigated.

It has been shown that cell mechanics is sensitive to their biological status, and changes in mechanical properties may strongly affect subsequent cellular functions.^{12–14} For example, penicillin binds to enzymes associated with peptidoglycan molecules in Gram-negative bacteria, which weakens the bacterial cell wall, and then leads to bacterial bursting due to intracellular osmotic pressure.¹² In plants, the growth capacity of the cell is regulated by cross-linking of peroxide-driven polysaccharides, because such cross-linking determines cell wall extension and stiffness.¹³ It is also known that the opening and closing of mechanosensitive channels can lead to structural as well as compositional changes in cellular membranes in prokaryotic cells.¹⁴ The mechanics of eukaryotic cells is very

important, but understanding and regulating their mechanical properties is much more complex than for prokaryotic cells.¹⁵ Recent studies reveal that in alveolar epithelial cells toxins such as thrombin or histamine lead to rapid and significant membrane stiffening, most likely due to reorganization of actin filaments (F-actin).^{16,17} It is also well-known that changes in the membrane cholesterol level alter the membrane fluidity and elastic modulus.^{12,18}

In many previous investigations on cell adhesion,^{4,5} and cell and vesicle mechanics,^{15,19,20} cell tracing dyes were frequently used as indicators of cell location, viability, and shape. It is important to verify if previously observed changes in cellular adhesion and mechanics are genuine properties of cells instead of side effects resulting from the addition of cellular tracing dyes. This work investigates the effect of cell tracing dyes on the mechanical properties of individual cells. Introduced in 2006 by our team,²¹ an atomic force microscopy (AFM) based single cell compression technique provides a very powerful means to investigate single cell mechanics. As schematically shown in Figure 1, a microsphere is attached to an AFM probe, and positioned above the center of a selected cell using a bright field objective. A force–deformation profile of this cell is then recorded by compressing the cell between the microsphere and the surface. While acquiring the force–distance curve, the cell deformation is monitored via optical or fluorescence microscopy. Such an experimental configuration enables direct and accurate force versus deformation measurements, which reveals cell mechanical responses arising primarily from the membrane and cytoskeleton. In contrast to other methods of measuring cell mechanics such as magnetic twisting cytometry²² or local AFM force mapping,¹⁵ AFM-based single cell compression probes *global* cell mechanics at the single cell level, over a full displacement range (0–100% or complete cell compression in most cases) with a wide force detection range (1 nN–50 μ N).

* To whom correspondence should be addressed. Fax: (530) 754-8557.
E-mail: liu@chem.ucdavis.edu.

[†] University of California.

[‡] University of California—Davis.

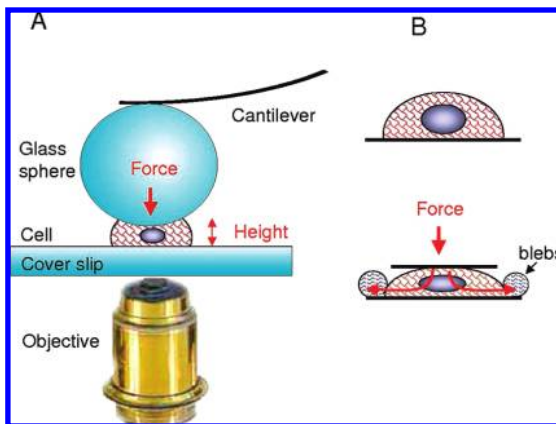


Figure 1. (A) Schematic diagram of single cell compression experiment. (B) Cell deformation under pressure such as cytoskeleton compression and blebbing. Red meshes represent cytoskeleton. Red arrows illustrate the concept of transducing external force into intracellular pressure.

The human breast cancer cell line, MDA-MB-468, was selected for this investigation because of their homogeneity in cellular geometry and properties. We verified that 90% of MDA-MB-468 cells exhibit the same mechanical properties within 20% precision for over 300 cells tested. Such consistency provides a good platform for investigating effects of external parameters, such as the introduction of dyes. The normal prostatic epithelial cell line MLC-SV40 was also utilized to verify the robustness of the findings.

Four cell tracing dyes were chosen to evaluate their impact on cell mechanics. Chloromethylfluorescein diacetate (CMFDA) is a long-term cell tracing dye, which provides sharp contrast between cells and media and exhibits bright and stable fluorescence.¹¹ Nonfluorescent CMFDA passes freely through the cellular membrane, and once inside, becomes fluorescent upon activation by intracellular enzymes. The chloromethyl group reacts with thiol-containing proteins to tag the cells.²³ The bright fluorescence and intracellular attachment make CMFDA an excellent probe for long-term studies on normal or transformed cells.¹¹ The effect of CMFDA on cell mechanical properties was compared with the short-term cell tracing dye Calcein Green AM. Like CMFDA, Calcein Green AM requires enzymes to activate its fluorescence. Unlike CMFDA, Calcein Green AM does not chemically bind to intracellular components.^{9,10} Other dyes used in the present work are chloromethyltetramethyl rhodamine (CMTMR) and carboxyfluorescein diacetate succinimidyl ester (CFDA-SE). CMTMR is a rhodamine derivative of the chloromethyl family of dyes, which follows activation pathways similar to those of CMFDA, but has a different fluorescence emission spectrum. CFDA-SE is the most widely used long-term tracing dye, which enters cells by diffusion and is then cleaved by intracellular esterase enzymes to form an amine-reactive product, CFSE.^{9,10} After cleavage, it produces a detectable fluorescence and covalently binds to the intracellular lysine residues and other amine-containing components; thus it is able to tag living cells for weeks.³

Our systematic investigation revealed that cell tracing dyes significantly increase cellular stiffness and cell-to-probe adhesion. Such stiffening may be quantified by extracting the Young's moduli of the cellular membrane and cytoskeleton using an analytical model derived from Hertzian mechanics and an elastic membrane theory. Attempts were also made to rationalize the observed changes in single cell mechanics. These observations should provide insight for researchers to consider

the effect of fluorescent dyes from their past and future investigations of cellular mechanics. The results also encourage the reexamination of prior investigations concerning single cell mechanics, if dyes were used.

Experimental Section

Cell Culture and Sample Preparation. Cells from the human mammary carcinoma cell line MDA-MB-468 were cultured in Dulbecco's modified Eagle's media (DMEM; GIBCO-BRL, Grand Island, NY) supplemented with 10% heat-inactivated fetal bovine serum (HyClone, Logan, UT), penicillin (100 U/mL), and streptomycin (100 µg/mL). Cells from the immortalized human prostatic epithelial cell line MLC-SV40²⁴ were maintained in keratinocyte serum-free medium (Invitrogen, Carlsbad, CA). Approximately 5×10^4 cells were seeded for 24 h onto the bottom of a Petri dish containing a glass coverslip (MatTek Corporation, Ashland, MA) prior to single cell mechanics measurements.

CMFDA, CMTMR, Calcein Green AM, and CFDA-SE dyes were all purchased from Invitrogen (Invitrogen, Carlsbad, CA). The uptake of cell tracing dyes follows standard procedures used in cellular biology and as recommended by the manufacturer.²³ Prior to labeling, cells were grown in a special kind of Petri dishes (each containing a glass bottom) for 24 h. Dyes were typically dissolved in prewarmed (37 °C) phosphate-buffered saline (PBS; pH 7.2) containing 1.2 µM dimethyl sulfoxide (DMSO; Fisher Scientific, Fairlawn, NJ) to reach 5 µM dye concentration. For labeling, cell media were removed and replaced with the dye-containing solution described above and incubated with it for 30 min. Then dye solution was replaced with fresh and warm media and incubated for another 30 min at 37 °C. Because trace amounts of DMSO were used to dissolve the dyes in these protocols, we also performed a secondary control sample using only DMSO treatment without dyes at the same final DMSO concentration of 1.2 µM. To investigate role of calcium ions in cell stiffening, MDA-MB-468 cells were incubated with 5 mM ethylene glycol tetraacetic acid (EGTA; Fisher Scientific, Fairlawn, NJ) for 30 min before compression.²⁵ All cell compression experiments were performed in specified culture media: Dulbecco's modified Eagle's media for MDA-MB-468 cells and keratinocyte serum-free media for MLC-SV40 cells.

Single Cell Mechanics. The experimental details of single cell compression setup were reported previously²¹ and are schematically shown in Figure 1. Cell deformation profiles were measured with the MFP-3D AFM (Asylum Research Corp., Santa Barbara, CA), which is equipped with a nanopositioning sensor for correcting the piezomanipulator's hysteresis and creeping. To guide the position of the microsphere directly above the center of designated cells, and to monitor the deformation of the cell upon force application, an inverted optical microscope IX50 with epifluorescent detection (Olympus America, Center Valley, PA) was combined with the AFM scanner. A standard Olympus FITC fluorescent cube and mercury lamp were used for fluorescent imaging. AC240 silicon cantilevers from Olympus with a standard force constant of $k = 2.0$ N/m were employed as a probe. Glass spheres with a diameter of 40 ± 2 µm (Duke Scientific, Fremont, CA) were attached to the apex of AFM tips using a premixed two-component epoxy (Elmer's epoxy resin, Columbus, OH). After sphere attachment, the spring constant was independently measured and calculated according to the added mass method,²⁶ and the results were in good agreement (within 15%) with values obtained from cantilever thermal noise measurements.^{27,28} Cell compression experiments were completed within 20 min after removal of the

TABLE 1: Comparison of Single Cell Mechanics for Untreated Cells (Control) and Cells Treated with Various Cell Tracing Dyes at Designed Concentrations

index	cell types	force (μN) at $\varepsilon = 0.3$	force (μN) at $\varepsilon = 0.8$	E_m (MPa)	E_c (kPa)	cell shape at high ε during compression	maximum adhesion to probe (μN)
1	MDA-MB-468	0.04–0.06	0.4–0.6	1.5–3.1	9–21	4–11 blebs	0.08–0.18
2	MDA-MB-468 with 5 μM CMFDA	0.1–0.15	2–2.7	10–17	17–33	4–10 blebs	0.1–0.69
3	MDA-MB-468 with 5 μM Calcein Green AM	0.22–0.46	2.8–3.6	14.6–17.9	34–51	8–12 blebs	0.12–0.64
4	MDA-MB-468 with 5 μM CFDA-SE	0.07–0.14	1.5–2.4	5.7–17	39–42	5–12 blebs	0.14–0.45
5	MDA-MB-468 with 5 μM CMTMR	0.07–0.17	1.7–3.5	6.9–13.2	13–17	5–11 blebs	0.45–0.88
6	MLC-SV40	0.03–0.06	0.3–0.6	1.7–4.9	13–26	5–10 blebs	0.01–0.16
7	MLC-SV40 with 5 μM CFDA-SE	0.07–0.17	1.7–2.5	12.1–15.1	61–67	4–10 blebs	0.15–0.42
8	MLC-SV40 with 5 μM Calcein Green AM	0.1–0.17	1.6–2.8	9.2–11.0	22–49	6–11 blebs	0.15–0.28
9	Jurkat Tl lymphoma cells	0.02–0.23	0.1–0.3	10–30	3–6	global bursting, no blebs	0.02–0.08

Petri dishes from the incubator to ensure the viability of the cells. To acquire cell compression profiles under incubator conditions, a special incubator was designed and assembled. Air, premixed with 5% CO₂ (Airgas, Woodland, CA), was flowing through this chamber which enclosed the AFM scanner and sample. Cells were heated to 37 ± 0.5 °C using a miniature resistance heater mounted directly on the glass Petri dish. Cell media temperature and internal incubator CO₂ concentration were monitored using calibrated STS-BTA and CO₂-BTA sensors, respectively (Vernier, Beaverton, OR).

Force–deformation profiles for single cell compression experiments were plotted as loading force versus relative cell deformation. Because the cell height of those uncompressed cells varies from 8 to 12 μm , relative deformation, $\varepsilon = \text{cell height change}/\text{initial cell height}$, is used to quantify the cell compression. The zero deformation for individual cells was determined from the point of the first detectable force (normally at 1–3 nN level) during the loading cycle.²¹ To avoid hydrodynamic forces, all cells were deformed at slow speed, 2 $\mu\text{m}/\text{s}$.²⁹ The load, F , applied to the cell is calculated from $F = k\Delta$, where k is the force constant of the sphere-modified AFM cantilever, and Δ represents the deformation of the cantilever.

Each cell compression event was recorded as a real movie by a Sony XC-ST50 monochrome camera (Edmund Optics, Barrington, NJ), attached to an inverted microscope. The snap shots from the movie can then be correlated with the corresponding points of the force profiles to reveal the cellular deformation at given force.

To ensure data reliability and reduce effect of cells' individuality, for each designed experimental condition at least two to three independent sets of measurements were performed. In each set 4–10 healthy cells were chosen to do force curves on, always in parallel with a similar number of control cells. This work reports results for single cell compression based on measurements of over 110 control cells in DMEM media, 30 control cells in DMEM media containing DMSO, 29 CMFDA labeled cells, 17 CMTMR labeled cells, 19 Calcein Green AM labeled cells, 14 CFDA-SE labeled cells, and 11 cells treated with EGTA for the MDA-MB-468 cell line. For the MLC-SV40 cell line, 29 control, 14 CMFDA labeled, 11 Calcein Green labeled, and 12 CFSE labeled cells were measured. Average values and standard deviations for force and Young's modulus in Table 1 were calculated using least-squares fitting of at least 10 typical force profiles. Cellular shape parameters, such as a cell's size, number, and size of blebs, were recorded by the video camera for each individual cell, and were averaged using 5–10 cells from different data sets.

Results

CMFDA Increases the Cellular Stiffness and Adhesion to Probes. First, we established the characteristic force profile for control cells and conducted extensive control experiments.

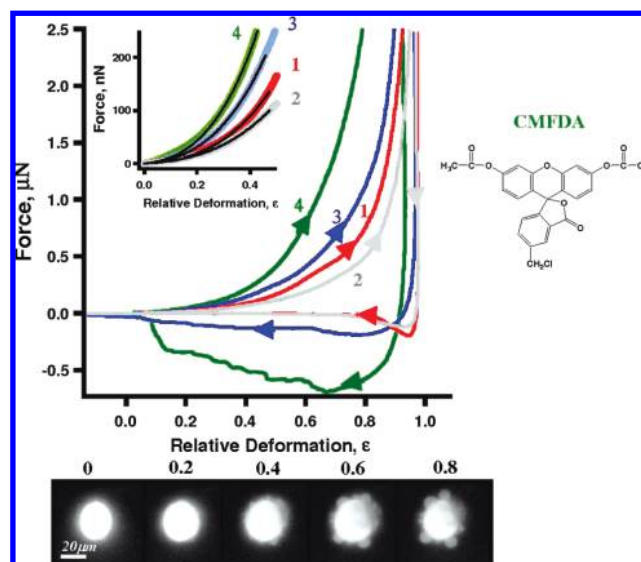


Figure 2. Typical profiles, i.e., force versus relative deformation, for the investigation of CMFDA dye effect on MDA-MB-468. Curve 1 (red) represents untreated cell, curve 2 (gray) is DMSO treated cell. Curves 3 (blue) and curve 4 (green) are deformation profiles for cell labeled with 3 and 5 μM CMFDA, respectively. Chemical structure of CMFDA is shown on the right. The inset shows the loading portion of the profile at low deformations. Bottom row includes epifluorescent snapshots of 5 μM CMFDA labeled MDA-MB-468 cell taken during compression cycle (bottom view), from which blebs are clearly visible.

Upon spreading on an unmodified glass coverslip, most MDA-MB-468 cells exhibit semispherical geometry with contact diameters of 15–20 μm . AFM compression experiments revealed heights of uncompressed living cells in the range 8–12 μm . A typical force–deformation profile for MDA-MB-468 control cells (curve 1, red) is shown in Figure 2, with 90% of cells following the same profile within 20%. The overall profile during the loading cycle (right-pointing triangles) is smooth without obvious stress peaks. The retreating cycle (left-pointing triangles) reveals an adhesive force (minimum in the curve) to be 185 nN. Among all control cells tested, the adhesion force ranges over 80–175 nN (Table 1, column 8). In contrast to macroscopic mechanics, the hysteresis on the force curve arises not only from energy dissipation during deformation but also from the adhesion forces between probe and cell upon contact. The area defined within the loading and unloading force profiles represents energy required in order to compress and then separate the probe from the cell (energy = $\int F \, dz$).

To rule out the perturbation due to DMSO addition, a second control experiment was carried out with cells subject to DMSO but without tracing dye (curve 2 in Figure 2). Approximately 75%

of DMSO treated cells follow the same profile within 25% of force values. The loading cycle for the majority of the population is similar to the control sample with a slight softening effect (probably due to the potential plasticization effect of DMSO). The retreating cycle of DMSO treated cells is almost superimposed with the control profile, with the adhesive force ranging over 80–160 nN. Additional control experiments include ambient versus incubator mechanics. No significant difference was observed in the loading part of the force–deformation profiles for cells compressed using the incubator (37 °C, 5% CO₂) and ambient conditions (25 °C, atmosphere 380 ppm CO₂). Unloading parts of the curves for compression in the incubator cells revealed much narrower adhesion peaks, but the maximum adhesion fell into the same values as the ambient experiments. Upon this validation, and to minimize the thermal drift and noise level of AFM due to implication of incubator, force–deformation profiles reported in this work were measured under ambient conditions in PBS or specified culture media.

The addition of CMFDA at a low concentration, 3 μM (Figure 2, curve 3), caused an increase in cell stiffness and adhesion; i.e., the loading cycle is above the control, and the retreat cycle exhibited longer range force and a slight increase in adhesion. At 5 μM, the changes are much more dramatic; i.e., curve 4 in Figure 2 is significantly above curve 1 (control) during loading, and below the control in the retreating part of the deformation cycle. The increase in the cell stiffness can be quantified by direct comparison of the forces at given deformations, as summarized in Table 1, columns 3 and 4. Typical MDA-MB-468 cells require 0.5 ± 0.1 μN force to be compressed by 80% (i.e., to 20% of its original height). Force values at 80% deformation reveal a 4–5 times increase in stiffening upon treating by 5 μM dye. Further increase in the dye concentration, up to 10 μM, does not lead to additional stiffening, possibly due to saturation.

As shown in the snapshots at the bottom of Figure 2, when deformation exceeds 50%, cells typically develop 4–10 membrane extrusions, or blebs, ranging from 4 to 12 μm in diameter. These are similar to the blebs occurring during apoptosis or cytokinesis.^{30,31} These blebs represent detachment of the plasma membrane from the cytoskeleton due to an increase in intracellular pressure driven by the external loading force. In contrast to a global expansion of the membrane, local blebbing (bubbling) is an indication of membrane heterogeneity, i.e., the result of local compositional and structural variations such as membrane protein, cholesterol, or lipid raft distribution.

Cell–microsphere adhesion is reflected in the retreating portion of the force–deformation profile. Following the convention of AFM force–distance curves,³² we define the minimum value at the retreating curve as the adhesive force. Comparing the retreat part of curve 4 with curve 1 (control) in Figure 2, it is clear that CMFDA dramatically increases cell adhesion. The adhesive force (130–640 nN) for the cells labeled with CMFDA is 1.5–5 times higher than that for the control (80–175 nN). The shape of the retractive part of the force curve indicates how the cell detaches from the probe. In contrast to control cells, where the probe detaches from the cell quickly upon retreating, the probe must be pulled up to initial cell height or further before detachment from labeled cells. Optical microscopy was performed during the force profiling, and it indicated that cells remained immobilized on the coverslip after separation. Therefore, retreating profiles measured the adhesion between the probe and the cells.

The observed impact of CMFDA is genuine because of well-controlled experiments completed as discussed above. To

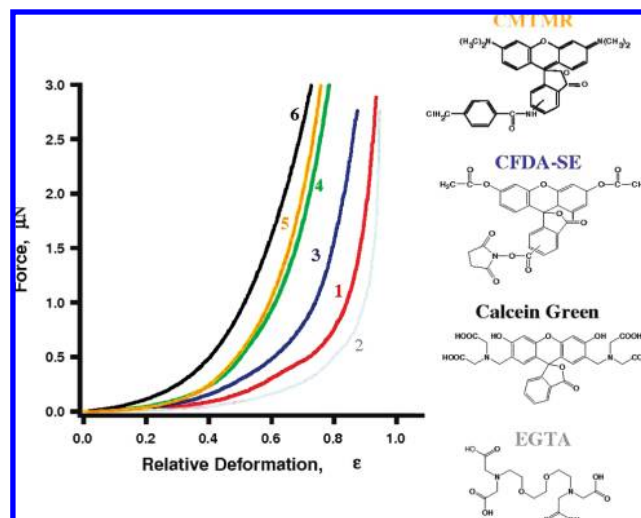


Figure 3. Typical force versus relative deformation profiles for MDA-MB-468 cells labeled with various dyes: a control cell (1, red), an EGTA treated cell (2, gray), and cells labeled with 5 μM CFDA-SE (3, blue), CMFDA (4, green), CMTMR (5, orange) and Calcein Green (6, black), respectively. The chemical structures of Calcein Green, EGTA, and CFDA-SE are shown on the right.

understand the mechanism of cell stiffening, the structure and functionality of CMFDA are provided to the right on Figure 2. According to previous studies, amphiphilic CMFDA molecules freely diffuse through the cellular membrane.¹¹ The molecules become fluorescent only after a hydrolysis reaction catalyzed by esterase, to conjugate all four aromatic rings.^{9,10} The chloromethyl group, –CH₂Cl, links to thiol-containing components such as cysteine, via glutathione S-transferase mediated reactions.²³ Since CMFDA has only one chloromethyl group, cross-linking of intracellular proteins should not have taken place.

Enhanced Stiffness and Adhesion Observed for All Four Cell Tracing Dyes Tested. A short-term cell tracing dye, Calcein Green AM, was also utilized for this investigation. Similar to CMFDA, Calcein Green AM becomes fluorescent intracellularly after hydrolysis reaction catalyzed by enzymes.^{9,10} Unlike CMFDA, Calcein Green AM does not covalently bind to proteins (see its molecular formula in Figure 3). The lack of strong binding functionality rationalizes the fact that Calcein Green AM remains inside the cell for 3–4 h instead of tens of days as in the case of CMFDA. Calcein Green AM is known to exert very little interference with leukocyte chemotaxis, superoxide production, or lymphocyte–target cell conjugation,³³ and is therefore considered to be a very gentle cell dye. Thus one may predict minimal perturbation to cell mechanics. However, the force–deformation profiles reveal the large increase in the single cell stiffness upon uptake of Calcein Green AM; i.e., the force–deformation profile is above all other profiles as shown in Figure 3, curve 6. It required 3.2 ± 0.4 μN to deform the MDA-MB-468 by 80%, in comparison to the 0.5 ± 0.1 μN in the case of control (see also Table 1, column 4). In other words, the cells become 6–7 times stiffer. The adhesion to the microsphere is also increased by 2–4 times, not as significant as the CMFDA. Similar to control cells, Calcein Green AM treated cells develop 4–10 blebs during compression.

To understand the mechanism of the effect of Calcein Green AM on cell mechanics, we first considered the possibility that Calcein Green AM affects the cell stiffness by reducing divalent metal concentrations, such as Ca²⁺. It was reported that reducing

extracellular Ca^{2+} concentration from 1.5 to 0.02 mM could double the stiffness.³⁴ Calcium ions are well-known to regulate many biological and cellular processes.¹² For example, a high Ca^{2+} concentration leads to muscle cell contraction.¹² Calcein Green AM has a listed application as a Ca^{2+} or Mg^{2+} indicator, but is rarely used in this fashion because its fluorescent intensity strongly depends on solution pH.³⁵ A stronger metal ion ligand, EGTA,²⁵ was used to explore the possibility that Calcein Green AM affects cell stiffness by reducing divalent metal concentration. Both Calcein Green and EGTA have four carboxylate and two amine groups in their structure. EGTA is widely used in experiments to sequester divalent ions by binding to metal ions via these four carboxylate and two amine groups. At 5 mM concentration, EGTA should decrease the intracellular Ca^{2+} level by 30–50%.²⁵ The force–deformation profile 2 in Figure 3 corresponds to cells treated with EGTA. In contrast to cell tracing dyes, EGTA decreases cellular stiffness by 30% without affecting adhesion. Similar to control cells, EGTA treated cells develop 4–10 blebs (4–12 μm in diameter) during compression. Therefore, a decrease of the intracellular calcium level is not responsible for the observed stiffening induced by Calcein Green AM.

The effect of cell stiffening upon adding another popular living cell dye, CFDA-SE, was also revealed. CFDA-SE is the most widely used probe for cell lineage tracking.²³ In transplanted cells, the signal of CFDA-SE can be traced in vivo for weeks.³ Similar to CMFDA, CFDA-SE enters cells by diffusion and is cleaved by intracellular esterase enzymes to become fluorescent CFSE.^{9,10} Its succinimidyl ester group covalently binds to the intracellular lysine residues and other amine-containing components.³ Curve 3 in Figure 3 shows a typical deformation profile for the cells treated with CFDA-SE. At 80% deformation 5 μM CFDA-SE increases MDA-MB-468 cell stiffness by 2–4 times (see Table 1, column 4). Probe-to-cell adhesion force also increases up to 3 times. During compression, CFDA-SE treated cells develop 5–12 blebs (4–12 μm in diameter) similar to control cells.

All three dyes, CMFDA, Calcein Green, and CFDA-SE, are based on the fluorescein molecule. The hypothesis that fluorescein and its derivatives play a key role in triggering cell stiffening and adhesion increase was invalidated using CMTMR, a rhodamine derivative of chloromethyl dyes.²³ The impact was similar to CMFDA: CMTMR increases cell stiffness by 4–7 times and probe-to-cell adhesion force by 4–6 times (see Table 1, column 8, and Figure 3, curve 5).

Enhanced Stiffening and Adhesion Are Observed for Other Cell Types. To investigate if cell stiffening induced by fluorescent dyes is limited only to one particular cell line, the normal human prostate cell line MLC-SV40 was employed for this single cell mechanics study. In contrast to MDA-MB-468, the human breast *cancer* cell line, MLC-SV40 is an immortalized *normal* human prostate cell line. Because MLC-SV40 cells have much wider size distribution than MDA-MB-468, only a subset of population with height 6–8 μm and lateral size 30–35 μm was chosen for cell mechanics studies.

Curve 1 in Figure 4 displays the deformation profiles for untreated (control) MLC-SV40 cells. Similarities in deformation profiles and blebbing behavior were observed in MLC-SV40 cells compared to MDA-MB-468 cells. For deformation exceeding 50%, MLC-SV40 cells develop typically 4–10 membrane extrusions, or blebs, 5–12 μm in diameter. The force profile during loading cycles for MLC-SV40 cells (right-pointing triangles) is smooth without obvious stress peaks. The retreating cycle (left-pointing triangles) reveals an adhesive force (mim-

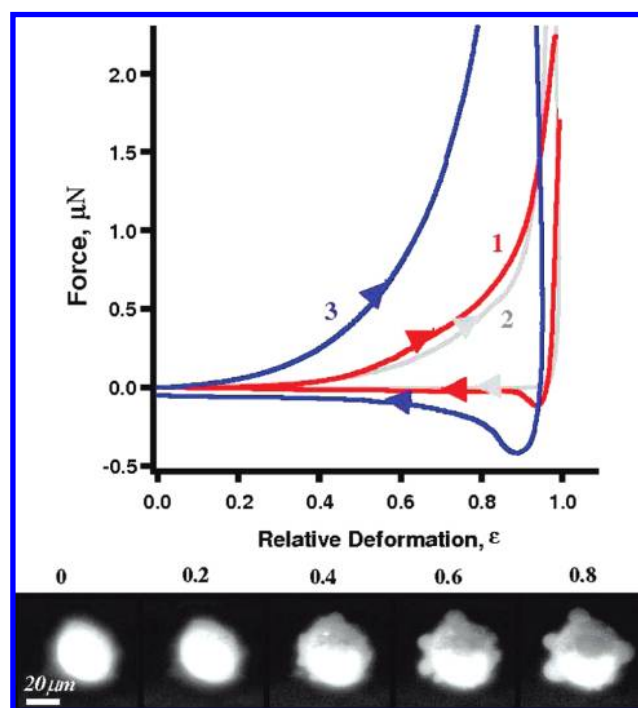


Figure 4. Typical deformation profiles for investigation of cell tracing dyes on MLC-SV40 cells: unlabeled (control) cell (1, red), DMSO treated cell (2, gray), and cell labeled with 5 μM CFDA-SE (3, blue). Bottom row shows epifluorescent snapshots of a 5 μM CFDA-SE labeled MLC-SV40 cell taken during compression cycle (bottom view).

imu) of 120 nN (see also Table 1, column 8). The DMSO addition softens control cells by 20% as shown as curve 2 in Figure 4, and diminishes the adhesion.

Cells treated with 5 μM CFDA-SE increased stiffness by 3–4 times. As shown in Figure 4, curve 3, $2.2 \pm 0.3 \mu\text{N}$ force is required to reach 80% deformation containing CFDA-SE, in comparison to the $0.4 \pm 0.1 \mu\text{N}$ in the case of control (also Table 1, column 4). The adhesion to the microsphere for MLC-SV40 cells is also increased by 2–4 times (Table 1, column 8). Similar to control cells, CFDA-SE treated cells develop 4–10 blebs 4–20 μm in diameter during compression. MLC-SV40 cells treated with Calcein Green AM also exhibit stiffness and adhesion increasing, as summarized in Table 1, column 8. Similar trends of dye-induced stiffening and higher probe-to-cell adhesion were observed for much softer cells, e.g., the N2A mouse neuroblastoma cell line. The fact that all three types of cells with totally different origins exhibit the same trends demonstrates the robustness of our findings.

Quantification of the Young's Moduli of Cellular Membrane and Cytoskeleton. A simple analytical model to quantify small cell deformations and extract membrane and cytoskeleton Young's moduli was derived from the elastic theory of membranes³⁶ and Hertzian contact mechanics.^{36,37} This model and derivation are based on the following assumptions: (a) prior to compression the single cell may be treated as a spherical membrane filled with an incompressible fluid and a gel-like cytoskeleton, sandwiched between the parallel plates; (b) at small deformations (*i.e.*, $\epsilon < 30\%$), the membrane (shell of balloon) is impermeable; (c) a cell's mechanical resistance arises from membrane stretching and cytoskeletal deformation with negligible contributions from other cellular components such as nuclei, during the initial compression process (*i.e.*, $\epsilon < 30\%$). Assumptions a–c can be understood as treating a cell as a nonpermeable balloon filled with fluid. More accurate models

and advance calculation methods such as finite element analysis would be necessary to account for profiles at high deformation as well as detailed heterogeneity of the membrane deformation.

Assumption a arises from fact that the probes are much larger than the equivalent sphere of cells under compression. MDA-MB-468 cells exhibit a hat shape on surfaces with contact diameter of 15–20 μm and height 8–12 μm . The probe's diameter is 40 μm . When compressing cells along the surface normal, the initial contact may be modeled as a 40 μm sphere compressing a small sphere ($D = 8\text{--}12 \mu\text{m}$, i.e., the cell height). Assumption b is based on large number of prior experiments^{12,31} as well as the single cell mechanics of T cells.²¹ During single cell compression, two characteristic behaviors, both consistent with membrane nonpermeability, were observed. The force–deformation profiles of T cells reveal stress peaks, corresponding to bursting of the membrane, as per simultaneous optical microscopy. This global membrane bursting happens because the intracellular pressure builds up during compression due to impermeability of the membrane. Instead of bursting, MDA-MB-468 and MLC-SV40 cells develop two to eight small blebs as a result of pressure buildup. This pressure-induced blebbing is very typical for many types of living cells³⁸ and is attributed to the behavior of nonpermeable plasma membranes under pressure, which causes membrane stretching and detachment from the cytoskeleton.³¹ It has been shown using M2 melanoma cells that cell volume remains constant during blebbing,^{30,31} which provides additional proof of membrane nonpermeability during blebbing. Therefore, regardless of global bursting or blebbing behavior, the impermeable balloon model remains valid under the conditions and time scale of our single cell compression experiment.

Assumption c is introduced to explain smooth deformation profiles of cells. Many adherent living cells such as keratinocyte, N2A, fibroblast (Lulevich, V.; Liu, G. Y., unpublished results) have smooth deformation profiles despite the appearance of blebs, which suggests other contributions (e.g., cytoskeleton) in addition to that of the membrane. At high deformation, the MDA-MB-468 cells' mechanics reflect mainly the behavior of their cytoskeleton, most likely F-actin and intermediate filaments.³⁹ Therefore the mechanical resistance of the cytoskeleton during cell compression can also be calculated using Hertzian contact mechanics.³⁶ The nuclear contribution is considered to be insignificant because of its location (frequently not under the probe) and the lack of significant Young's modulus contrast between the cytoskeleton and nucleus.⁴⁰

A simple analytical expression can be derived, under assumptions a–c, to account for the cell deformation profiles (see the Appendix for the detailed mathematical derivation):

$$F = F_{\text{membrane}} + F_{\text{cytoskeleton}} = 2\pi \frac{E_m}{1 - \nu_m} h R_0 \epsilon^3 + \pi \frac{\sqrt{2} E_c}{3(1 - \nu_c^2)} R_0^2 \epsilon^{3/2} \quad (1)$$

where ϵ is the relative deformation of the cell; R_0 and h are the radius of the uncompressed cell and its plasma membrane thickness; E_m and E_c represent the Young's moduli of the membrane and the cytoskeleton, respectively; ν_m and ν_c represent the Poisson ratios of the membrane and the cytoskeleton, respectively. Equation 1 reveals that cellular mechanical resistance arising from cytoskeletal compression follows a $F \propto E_c \epsilon^{3/2}$ relationship, and a $F \propto E_m \epsilon^3$ term from the membrane stretching. The fact that the deformation profiles for the membrane and cytoskeleton follow different power laws (cubic

vs 2/3) allows us to extract E_m and E_c from one cell compression profile using nonlinear fitting.

Prior to the fitting, key values in eq 1 are determined: (a) membrane thickness is estimated to be 4 nm; (b) R_0 equals half the cell height; (c) a Poisson ratio of $\nu = 1/2$ is used for the cell membrane (i.e., incompressible); (d) the Poisson ratio of the cytoskeleton is $\nu = 0$, fully compressible material. Note that the ν value of the cytoskeleton contribution depends on membrane–cytoskeleton interactions. For a detached cytoskeleton, our assumption $\nu = 0$ is accurate. For a strongly attached membrane, lateral cytoskeleton extension may occur during compression, which would result in a higher effective ν_c , between 0 and 0.5. A much more complex model is needed to account for such a cytoskeletal extension. However, due to the mathematical expression $1/(1 - \nu^2)$, derived from the Hertzian model, $\nu = 0.25$ (very sticky cytoskeleton to membrane) would only affect the calculation by 6%, which is insignificant. Thus we proceed with $\nu = 0$ in this initial effort to quantify the force profile.

As shown in the inset in Figure 2, the fitting is excellent at deformations up to 50%. In the case of the control of MDA-MB-468 cells, Young's modulus is $3.03 \pm 0.08 \text{ MPa}$ for the membrane, and $9.6 \pm 0.4 \text{ kPa}$ for the cytoskeleton.

Quantitative results for all experiments are summarized in Table 1. One may attain experimental force values from the curves shown in Figures 2–4. Columns 2 and 3 in Table 1 provide a comparison of two points: 30% (low) and 80% (high) deformations, respectively. Columns 5 and 6 list the Young's modulus for the membrane and the cytoskeleton, respectively, which enables quantification of cell stiffening; e.g., a typical MDA-MB-468 cell treated with 5 μM CMFDA became 4–7 times harder in the membrane and 1–3 times stiffer in the cytoskeleton. The most dramatic E_m and E_c increases were observed when MDA-MB-468 cells were treated with 5 μM Calcein Green AM: E_m increased by 6.3–7.8 times and E_c by 2.3–3.4 times. The dye impact on MLC-SV40 cells was not as significant as for MDA-MB-468 cells. For instance, an average MLC-SV40 cell treated with 5 μM CFDA-SE exhibits a 3.7–4.6 times increase in E_m and 3.1–3.3 times higher in E_c .

The quantitative analysis enables the separation of the impact: dye molecules strongly affect both the cytoskeleton and the membrane; however, the increase in membrane Young's modulus is more dramatic, up to 8 times greater. This change is significant in cellular biology and tissue engineering. For example, well-known thrombin and histamine induced cell stiffening increases epithelial cell rigidity only by 1.2–2 times.¹⁷ In tissue engineering applications, designed scaffolds must match cellular mechanics to facilitate cell proliferation; thus a factor of 8 is certainly a significant quantity.⁴¹

Discussion

We hope to provide a rationalization of the observed effect of cell tracing dyes on single cell mechanics from our investigation as well as the knowledge of cellular structure and biochemistry. Evidence of this investigation includes (a) significant change in the cell-to-probe adhesion and (b) significant increase of Young's moduli of the cellular membrane and of cytoskeleton upon addition of cell tracing dyes.

Change in the cell-to-probe adhesion for labeled cells suggests that the cellular surface changes dramatically upon addition of cell tracing dye. The dye molecules consist of aromatic rings with hydrophilic groups; therefore, these molecules may be incorporated into the lipid bilayer as well as diffuse through the cellular membrane. The lipophilic portion of the dye

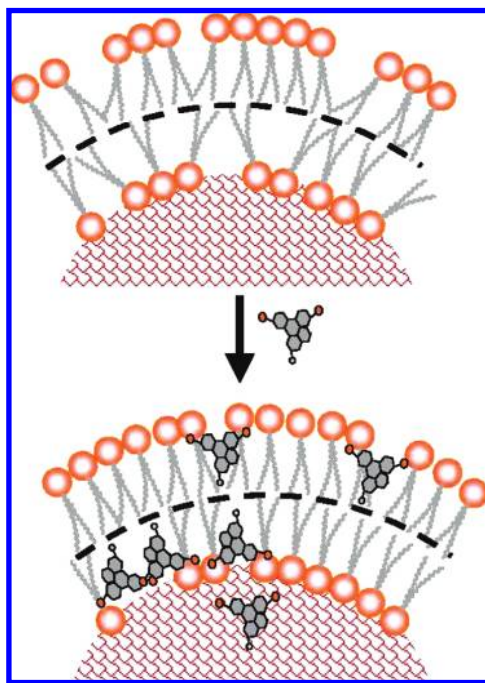


Figure 5. Schematic diagram of how CMFDA cell tracing dye molecules can incorporate into phospholipid bilayer, increasing its rigidity. Polar regions are shown in orange, nonpolar regions are shown in gray, and cytoplasm is represented by red mesh.

molecules can interact favorably with phospholipid-based cellular membranes, especially at domain boundaries. It has been shown earlier that lipophilic dye molecules are not only incorporated into lipid membranes and vesicles, but also form complexes and domains.⁴² The existence of such domains changes the physical properties of the lipid bilayer such as its mobility, rigidity, and phase transition kinetics.^{42,43} These dyes have chemical functionalities similar to the cell tracing dyes used for this investigation; therefore, one may postulate that the dye–membrane interactions in our case are also very strong. It is also known that eukaryotic plasma membrane stiffness, fluidity, and integrity are regulated by cholesterol.^{12,44,45} The hydroxyl group of cholesterol forms hydrogen bonds with polar phospholipid head groups, and the hydrophobic part of the cholesterol molecule interacts with the hydrocarbon tails of phospholipids, thus decreasing the mobility.¹² The structure and amphiphilicity of the cell tracing dye molecules exhibit similarities to cholesterol molecules, thus likely having a similar impact on the membrane structure and properties.

Taken collectively, we propose a schematic rationalization of cell–dye interaction, as illustrated in Figure 5. This illustration suggests that the change of cell mechanical properties upon adding cell tracing dyes is primarily due to the incorporation of amphiphilic dye molecules into cellular plasma membranes and their interactions with molecules in the lipid bilayers. These interactions increase the rigidity of the lipid bilayer, thus leading to the increase in its Young's moduli. The formation of larger domains of similar functionality as a result of dye incorporation is likely due to the accumulation of hydrophilic domains in a more steady manner, thus manifesting in the higher adhesion to glass spheres terminated by hydroxyl groups. This is analogous to previous observations that fluorescent dyes such as CFDA-SE, DiL, and Calcein Green increase cell adhesion to glass surfaces.⁴

Detailed molecular mechanisms of cell stiffening and adhesion increase would require molecular resolution tools in

conjunction with single cell compression to prove our hypothesis that changes in cell mechanics are due to incorporation of the dye into the lipid membrane. Cell tracing dyes are very frequently utilized in cellular biology research because they provide highly sensitive fluorescent tags without compromising cellular functions such as growth and proliferation. In many investigations concerning cellular adhesion and mechanics, fluorescent dyes have also been utilized frequently without knowledge of the potential impact on the outcome of the investigation. This initial and systematic investigation should not only warn researchers who use cell tracing dyes while studying cell mechanical properties, but may have direct applications in cellular biology. For example, the dramatic dye-induced cell stiffening effect, observed here for the first time, can be used to increase the stiffness of living cells to make them suitable for high-resolution AFM imaging without fixation. Changes in cellular adhesion can also be utilized for cell immobilization. Hopefully these advantages will benefit cellular research further in the future.

Acknowledgment. We thank Drs. Huan-Yuan Chen and Fu-Tong Liu for providing the Jurkat T cells and Drs. Lee-Way Jin and Hyun-Seok Hong and Mr. Chris Zimmer for N2A mouse neuroblastoma cells. Dr. Christopher Koehler is gratefully acknowledged for his assistance with manuscript preparation. This work was supported by the University of California at Davis, The National Science Foundation (DMR0421521 and DMR0723118), and the National Institutes of Health (R21GM77850-01).

Appendix

In our model, prior to compression the living cell mechanical structure is approximated as a spherical impermeable elastic balloon (spherical membrane). This balloon is filled with an incompressible fluid and gel-like materials.

Calculation of fluid-filled impermeable spherical membrane deformation between parallel plates assumes that under small deformations the lateral part of the membrane extends spherically (except contact regions).⁴⁶ Then, using the volume conservation, the lateral radius of the membrane after deformation, R , can be calculated from the initial membrane radius R_0 and relative deformation ε :

$$R = R_0 + \frac{R_0}{2} \varepsilon^2 \quad (\text{A1})$$

The energy of the stretching of the membrane G with thickness h according to elastic theory is

$$G = \frac{h}{2} \int u_{\alpha\beta} \sigma_{\alpha\beta} dS \quad (\text{A2})$$

where integration is over membrane surface, $u_{\alpha\beta}$ is two-dimensional deformation, and $\sigma_{\alpha\beta}$ is a two-dimensional deformation stress tensor:

$$\sigma_{\alpha\beta} = \frac{E_m}{1 - \nu_m^2} [(1 - \nu) u_{\alpha\beta} + \nu \delta_{\alpha\beta} u_{\gamma\gamma}] \quad (\text{A3})$$

where E_m is Young's modulus, ν_m is the Poisson ratio of the membrane, and the summation must be over repeating indices.

Balance of stress defines the pressure inside the balloon:

$$P = \frac{h}{R} (\sigma_{\theta\theta} + \sigma_{\phi\phi}) \quad (\text{A4})$$

Using the relation between stress and deformation tensors

$$\begin{aligned} Eu_{\theta\theta} &= \sigma_{\theta\theta} - \nu\sigma_{\phi\phi} \\ Eu_{\phi\phi} &= \sigma_{\phi\phi} - \nu\sigma_{\theta\theta} \end{aligned} \quad (\text{A5})$$

and the assumption that the deformed balloon has a spherical shape, yields

$$u_{\phi\phi} = u_{\theta\theta} = \frac{u_r}{r} = \frac{r - r_0}{r_0} \quad (\text{A6})$$

and the stress tensors

$$\sigma_{\phi\phi} = \sigma_{\theta\theta} = \frac{E_m}{1 - \nu} \frac{r - r_0}{r_0} \quad (\text{A7})$$

Substituting eqs A6 and A7 into eq A2, we obtain the elastic energy of the spherical membrane stretching:

$$G_{\text{el}} \approx 4\pi \frac{E_m}{1 - \nu_m} (r - r_0)^2 \quad (\text{A8})$$

Correspondingly, the reaction force (load)

$$F_{\text{el}} = -\frac{\partial G_{\text{el}}}{\partial Z} = 2\pi \frac{E_m}{1 - \nu_m} h R_0 \epsilon^3 \quad (\text{A9})$$

has cubic dependence on the relative deformation ϵ .

Note that membrane bending was ignored. For bending of the noncontact area of a spherical membrane, the bending contribution is proportional to $(h/R)^2$.³⁶ For a typical cellular membrane of $R = 5 \mu\text{m}$ and $h = 4 \text{ nm}$, h/R is less than 10^{-6} and can thus be neglected. However, strong membrane bending does occur at the contact region. The change from the membrane in contact with the substrate to the free membrane, at the contact angle θ , happens over a length comparable to the membrane thickness. Then the local radius of curvature of the membrane near the separation line can be estimated as $\rho = h/\theta$. The elastic energy of bending used from beam theory is

$$G_b \approx \frac{E_m I h l}{2 \rho^2} \quad (\text{A10})$$

where $I = h^3/12$ is the second momentum of the area of the contact, and $l = 4\pi r \sin \theta \approx 4\pi r \theta$ is the total length of contact. Substituting l and I back to the expression of the bending energy (eq A10), and taking into account the volume conservation requirement $R - R_0 \approx (R_0 \theta^4)/8$, we obtain:

$$G_b \approx \frac{\sqrt{2}\pi}{3} E_m h^2 R_0 \epsilon^{3/2} \quad (\text{A11})$$

The force due to contact area bending therefore equals

$$F_b = -\frac{\partial G_b}{\partial Z} = \frac{\pi}{2\sqrt{2}} E_m h^2 \epsilon^{1/2} \quad (\text{A12})$$

The ratio between the bending and stretching terms can be calculated using eqs A9 and A12:

$$\frac{F_{\text{bending}}}{F_{\text{stretching}}} \approx \frac{h}{R_0} \frac{1}{\epsilon^{5/2}} \quad (\text{A13})$$

Given that the lipid bilayer thickness (h) is typically 4 nm, while the cell radius is above $5 \mu\text{m}$, at $\epsilon = 0.1 - 0.3$, this ratio is below 0.05. Therefore, one can neglect the bending deformation contribution, and use eq A9 to estimate the fluid-filled impermeable spherical membrane's deformation.

Cytoskeletal compression can be estimated using contact Hertz theory. Assuming that glass is much harder than the cell and has an infinite radius of curvature, the deformation of the

cytoskeleton compressed between two parallel plates can be calculated using³⁶

$$F_c = \frac{\sqrt{2}E_c}{3(1 - \nu_c^2)} R_0^2 \epsilon^{3/2} \quad (\text{A14})$$

where R_0 represents the cell contact radius before deformation and E_c and ν_c are the Young's modulus and Poisson ratio of the cytoskeleton, respectively.

Therefore superposition of eqs A9 and A14 gives overall cell deformation in estimation as

$$F = \frac{\sqrt{2}E_c}{3(1 - \nu_c^2)} R_0^2 \epsilon^{3/2} + 2\pi \frac{E_m}{1 - \nu} h R_0 \epsilon^3 \quad (\text{A15})$$

where the first term arises from the cytoskeleton compression resistance and is responsible for global membrane stretching, and membrane-to-cytoskeleton attachment is neglected.

Symbols

E_m = Young's modulus of membrane

E_c = Young's modulus of cytoskeleton

F = force

R_0 = radius of the uncompressed cell

ϵ = relative deformation

ν_m = Poisson ratio of membrane

ν_c = Poisson ratio of cytoskeleton

References and Notes

- Lichtenfels, R.; Biddison, W. E.; Schulz, H.; Vogt, A. B.; Martin, R. Care-lass (calcein-release-assay), an improved fluorescence-based test system to measure cytotoxic T-lymphocyte activity. *J. Immunol. Methods* **1994**, *172* (2), 227–239.
- Wang, X. M.; Terasaki, P. I.; Rankin, G. W.; Chia, D.; Zhong, H. P.; Hardy, S. A new microcellular cytotoxicity test based on calcein AM release. *Hum. Immunol.* **1993**, *37* (4), 264–270.
- Lyons, A. B. Divided we stand: Tracking cell proliferation with carboxyfluorescein diacetate succinimidyl ester. *Immunol. Cell Biol.* **1999**, *77* (6), 509–515.
- Declerck, L. S.; Bridts, C. H.; Mertens, A. M.; Moens, M. M.; Stevens, W. W. J. Use of fluorescent dyes in the determination of adherence of human-leukocytes to endothelial-cells and the effect of fluorochromes on cellular function. *J. Immunol. Methods* **1994**, *172* (1), 115–124.
- Vankessel, K. P. M.; Park, C. T.; Wright, S. D. A fluorescence microassay for the quantitation of integrin-mediated adhesion of neutrophil. *J. Immunol. Methods* **1994**, *172* (1), 25–31.
- Bischof, J. C.; Padanilam, J.; Holmes, W. H.; Ezzell, R. M.; Lee, R. C.; Tompkins, R. G.; Yarmush, M. L.; Toner, M. Dynamics of cell-membrane permeability changes at supraphysiological temperatures. *Bioophys. J.* **1995**, *68* (6), 2608–2614.
- Scorrano, L.; Petronilli, V.; Di Lisa, F.; Bernardi, P. Commitment to apoptosis by GD3 ganglioside depends on opening of the mitochondrial permeability transition pore. *J. Biol. Chem.* **1999**, *274* (32), 22581–22585.
- Homolya, L.; Hollo, Z.; Germann, U. A.; Pastan, I.; Gottesman, M. M.; Sarkadi, B. Fluorescent cellular indicators are extruded by the multidrug-resistance protein. *J. Biol. Chem.* **1993**, *268* (29), 21493–21496.
- Bruning, J. W.; Kardol, M. J.; Arentzen, R. Carboxyfluorescein fluorochromasia assays. 1. Non-radioactively labeled cell-mediated lympholysis. *J. Immunol. Methods* **1980**, *33* (1), 33–44.
- Jones, K. H.; Senft, J. A. An improved method to determine cell viability by simultaneous staining with fluorescein diacetate propidium iodide. *J. Histochem. Cytochem.* **1985**, *33* (1), 77–79.
- Lantz, R. C.; Lemus, R.; Lange, R. W.; Karol, M. H. Rapid reduction of intracellular glutathione in human bronchial epithelial cells exposed to occupational levels of toluene diisocyanate. *Toxicol. Sci.* **2001**, *60* (2), 348–355.
- Karp, G. *Cell and molecular biology*; John Wiley & Sons Inc.: New York, 2003; p 785.
- Zarra, I.; Sanchez, M.; Queijeiro, E.; Pena, M. J.; Revilla, G. The cell wall stiffening mechanism in *Pinus pinaster* Aiton: regulation by apoplastic levels of ascorbate and hydrogen peroxide. *J. Sci. Food Agric.* **1999**, *79* (3), 416–420.
- Perozo, E. Gating prokaryotic mechanosensitive channels. *Nat. Rev. Mol. Cell Biol.* **2006**, *7* (2), 109–119.

- (15) Suresh, S. Biomechanics and biophysics of cancer cells. *Acta Biomater.* **2007**, *3*, 413–438.
- (16) Bausch, A. R.; Hellerer, U.; Essler, M.; Aepfelbacher, M.; Sackmann, E. Rapid stiffening of integrin receptor–Actin linkages in endothelial cells stimulated with thrombin: A magnetic bead microrheology study. *Biophys. J.* **2001**, *80* (6), 2649–2657.
- (17) Trepot, X.; Grabulosa, M.; Buscemi, L.; Rico, F.; Farre, R.; Navajas, D. Thrombin and histamine induce stiffening of alveolar epithelial cells. *J. Appl. Physiol.* **2005**, *98* (4), 1567–1574.
- (18) Evans, E.; Needham, D. Physical properties of surfactant bilayer-membranes—thermal transitions, elasticity, rigidity, cohesion, and colloidal interactions. *J. Phys. Chem.* **1987**, *91* (16), 4219–4228.
- (19) Peeters, E. A. G.; Oomens, C. W. J.; Bouten, C. V. C.; Bader, D. L.; Baaijens, F. P. T. Viscoelastic properties of single attached cells under compression. *J. Biomech. Eng.: Trans ASME* **2005**, *127* (2), 237–243.
- (20) Ratanabanangkoon, P.; Gropper, M.; Merkel, R.; Sackmann, E.; Gast, A. P. Mechanics of streptavidin-coated giant lipid bilayer vesicles: A micropipet study. *Langmuir* **2003**, *19* (4), 1054–1062.
- (21) Lulevich, V.; Zink, T.; Chen, H. Y.; Liu, F. T.; Liu, G. Y. Cell mechanics using atomic force microscopy-based single-cell compression. *Langmuir* **2006**, *22* (19), 8151–8155.
- (22) Hoffman, B. D.; Massiera, G.; Van Citters, K. M.; Crocker, J. C. The consensus mechanics of cultured mammalian cells. *Proc. Natl. Acad. Sci. U.S.A.* **2006**, *103* (27), 10259–10264.
- (23) Cell tracker probes for long-term tracing of living cells. <http://probes.invitrogen.com/>.
- (24) Lee, M. S.; Garkovenko, E.; Yun, J. S.; Weijerman, P. C.; Peehl, D. M.; Chen, L. S.; Rhim, J. S. Characterization of adult human prostatic epithelial-cells immortalized by Polybrene-induced DNA transfection with a plasmid containing an origin-defective SV40-genome. *Int. J. Oncol.* **1994**, *4* (4), 821–830.
- (25) Brunner, F. Dependence of Endothelin-1 secretion on Ca²⁺. *Biochem. Pharmacol.* **1995**, *49* (12), 1785–1791.
- (26) Cleveland, J. P. M.; Bocek, D.; Hansma, P. K. A nondestructive method for determining the spring constant of cantilevers. *Rev. Sci. Instrum.* **1993**, *64* (2), 403–405.
- (27) Walters, D. A.; Cleveland, J. P.; Thomson, N. H.; Hansma, P. K.; Wendman, M. A.; Gurley, G.; Elings, V. Short cantilevers for atomic force microscopy. *Rev. Sci. Instrum.* **1996**, *67* (10), 3583–3590.
- (28) Butt, H. J.; Jaschke, M. Calculation of the thermal noise in Atomic Force Microscopy. *Nanotechnology* **1995**, *6* (1), 1–7.
- (29) Lulevich, V. V.; Vinogradova, O. I. Effect of pH and salt on the stiffness of polyelectrolyte multilayer microcapsules. *Langmuir* **2004**, *20* (7), 2874.
- (30) Charras, G. T.; Hu, C. K.; Coughlin, M.; Mitchison, T. J. Reassembly of contractile Actin cortex in cell blebs. *J. Cell Biol.* **2006**, *175* (3), 477–490.
- (31) Charras, G. T.; Yarrow, J. C.; Horton, M. A.; Mahadevan, L.; Mitchison, T. J. Non-equilibration of hydrostatic pressure in blebbing cells. *Nature (London)* **2005**, *435* (7040), 365–369.
- (32) Ducker, W. A.; Senden, T. J.; Pashley, R. M. Direct measurement of colloidal forces using an atomic force microscope. *Nature (London)* **1991**, *353*, 239–41.
- (33) Means, T. L.; Geroski, D. H.; Lhernault, N.; Grossniklaus, H. E.; Kim, T.; Edelhauser, H. F. The corneal epithelium after Optisol-GS storage. *Cornea* **1996**, *15* (6), 599–605.
- (34) Beurg, M.; Nam, J. H.; Crawford, A.; Fettiplace, R. The actions of calcium on hair bundle mechanics in mammalian cochlear hair cells. *Biophys. J.* **2008**, *94* (7), 2639–2653.
- (35) Breuer, W.; Epsztajn, S.; Millgram, P.; Cabantchik, I. Z. Transport of iron and other transition-metals into cells as revealed by a fluorescent probe. *Am. J. Physiol.—Cell Physiol.* **1995**, *269* (6), C1354–C1361.
- (36) Landau, L. D.; Lifshits, E. M. *Theory of elasticity*, 3rd ed.; 1965; p 202.
- (37) *Cytoskeletal mechanics*; Mofrad, M. R. K., Kamm, R. D., Eds.; Cambridge University Press: New York, 2006; p 244.
- (38) Peeters, E. A. G.; Oomens, C. W. J.; Bouten, C. V. C.; Bader, D. L.; Baaijens, F. P. T. Mechanical and failure properties of single attached cells under compression. *J. Biomech.* **2005**, *38* (8), 1685–1693.
- (39) Fuchs, E. The cytoskeleton and disease: Genetic disorders of intermediate filaments. *Annu. Rev. Genet.* **1996**, *30*, 197–231.
- (40) Dahl, K. N.; Engler, A. J.; Pajerowski, J. D.; Discher, D. E. Power-law rheology of isolated nuclei with deformation mapping of nuclear substructures. *Biophys. J.* **2005**, *89* (4), 2855–2864.
- (41) Langer, R.; Vacanti, J. P. Tissue engineering. *Science* **1993**, *260* (5110), 920–926.
- (42) Williamson, P.; Mattocks, K.; Schlegel, R. A. Merocyanine-540, a fluorescent probe sensitive to lipid packing. *Biochim. Biophys. Acta* **1983**, *732* (2), 387–393.
- (43) Langner, M.; Hui, S. W. Merocyanine interaction with phosphatidylcholine bilayers. *Biochim. Biophys. Acta* **1993**, *1149* (1), 175–179.
- (44) Byfield, F. J.; Aranda-Espinoza, H.; Romanenko, V. G.; Rothblat, G. H.; Levitan, I. Cholesterol depletion increases membrane stiffness of aortic endothelial cells. *Biophys. J.* **2004**, *87* (5), 3336–3343.
- (45) Sun, M.; Northup, N.; Marga, F.; Huber, T.; Byfield, F. J.; Levitan, I.; Forgacs, G. The effect of cellular cholesterol on membrane cytoskeleton adhesion. *J. Cell Sci.* **2007**, *120* (13), 2223–2231.
- (46) Lulevich, V.; Andrienko, D.; Vinogradova, O. I. Elasticity of polyelectrolyte multilayer microcapsules. *J. Chem. Phys.* **2004**, *120* (8), 3822.

JP8103358